JOURNAL OF THERMOPHYSICS AND HEAT TRANSFER
Vol. 31, No. 4, October–December 2017

Multitemperature Dissociation Rate of $N_2 + N_2 \rightarrow N_2 + N + N$ Calculated Using Selective Sampling Quasi-Classical Trajectory Analysis

Stephen Voelkel* and Philip L. Varghese†
University of Texas at Austin, Austin, Texas 78712
and
Venkat Raman‡
University of Michigan, Ann Arbor, Michigan 48109

DOI: 10.2514/1.T5103

The dissociation rate of nitrogen for the reaction $N_2 + N_2 \rightarrow N_2 + N + N$ was calculated as a function of a translational, vibrational, and rotational temperature, each ranging from 6000 to 60,000 K. The rate coefficients were calculated using quasi-classical trajectory analysis, in which approximately 5.35 billion trajectories were directly simulated. Furthermore, a new selective sampling procedure was implemented so that only trajectories with sufficient energy to cause dissociation were sampled. At 6000 K, this method reduced the computational cost by nearly two orders of magnitude. Finally, the set of rate coefficients was used to extend the two-temperature model conventionally used in computational-fluid-dynamics simulations. For temperatures between 13,000 and 40,000 K, where rotational energy of N_2 should be independently modeled, the fit shows good agreement with the quasi-classical trajectory-calculated rate coefficients.

Nomenclature

b	=	impact parameter, Å
c	=	effective temperature coefficients
E_d	=	dissociation energy of N_2, J
E_{rv}	=	total rovibrational energy of both reactants, J
f_g	=	relative speed probability distribution function
f_r	=	rotational state probability distribution function
f_{rv}	=	rovibrational state probability distribution function
f_v	=	vibrational state probability distribution function
f_τ	=	reactant phase probability distribution function
g	=	relative translational speed, Å/fs
g_s	=	spin degeneracy
g_o	=	minimum relative translational speed, Å/fs
J	=	rotational quantum number
k_B	=	Boltzmann constant, J/K
k_d	=	thermal nonequilibrium dissociation rate coefficient, $cm^3/(s \cdot mol)$
k_d^{eq}	=	thermal equilibrium dissociation rate coefficient, $cm^3/(s \cdot mol)$
k_d^P	=	Park's model dissociation rate coefficient, $cm^3/(s \cdot mol)$
k_d^{ref}	=	reference thermal nonequilibrium dissociation rate coefficient, $cm^3/s \cdot mol$
M_2	=	total mass of second reactant, kg
N	=	number of simulated trajectories
N_d	=	number of dissociative trajectories
N_{eff}	=	number of effective trajectories
$\boldsymbol{n}$	=	initial rovibrational state
P_d	=	probability of dissociation
Q_{rv}	=	rovibrational partition function
Q_v	=	vibrational partition function
T	=	temperature, K
T_e	=	effective temperature, K
T_r	=	rotational temperature, K
T_t	=	translational temperature, K
T_v	=	vibrational temperature, K
v	=	vibrational quantum number
δ_d	=	trajectory outcome
ε	=	statistical relative uncertainty
η	=	normalization factor
μ	=	reduced mass, kg
ξ	=	minimum speed factor
σ_d	=	dissociation cross section, $Å^2$
$\boldsymbol{\tau}$	=	initial phase of reactants

Received 28 September 2016; revision received 7 February 2017; accepted for publication 18 March 2017; published online 25 May 2017.

*Graduate Student, Institute for Computational Engineering and Sciences. Student Member AIAA.
†Professor, Department of Aerospace Engineering and Engineering Mechanics. Senior Member AIAA.
‡Associate Professor, Department of Aerospace Engineering. Senior Member AIAA.

I. Introduction

DISSOCIATION of air is an important process that is vital to the design of hypersonic vehicles. In high-speed reentry, the thermochemical conditions behind the shocks created by the vehicle can readily cause nitrogen and oxygen molecules to dissociate. The interaction of the products with the vehicle, including recombination on the surface, can affect thermal loads as well as the development of the boundary layer [1–3]. In addition to understanding the physics of such reactions, developing reliable chemical rate coefficient models is necessary for performing high-fidelity computational fluid dynamics (CFD) calculations that can aid the vehicle design process. For this reason, much work has been done to model rotational and vibrational nonequilibrium effects in high-temperature air flows [4–26].

In general, it is known that the dissociation rate coefficients are a strong function of the thermal nonequilibrium that exists at these conditions. By this, it is meant that the internal modes of the constituent molecules are not at equilibrium. To incorporate these effects, a reliable description of thermal nonequilibrium is needed in the CFD approach. Here, many models are available [4–11,17,21,23,27–32]. The most comprehensive description will require the solution of a transport equation for the population of molecules in each rovibrational state, which is the equivalent of a spatially inhomogeneous master equation [15,17,33–35]. At the same time, rates that describe the transitions between the different rovibrational states, the state-specific rate coefficients, will be required [12,17,22,33,36–39]. For N_2–O_2 systems under this description, an additional $\mathcal{O}(10^4)$ transport equations would

need to be solved alongside the CFD simulation (one for each rovibrational state), making full-scale simulations intractable. In most practical applications, a state-averaged approach is used [7–9,16,23,29,30,40], which invokes a multitemperature description. Here, each internal mode (i.e., vibrations, rotations, and translations) are individually assumed to be at equilibrium, but at different temperatures, leading to mode-specific temperatures denoted as vibrational (T_v), rotational (T_r), and translational (T_t) temperatures. In the CFD code, transport equations for these temperatures (or more generally, the associated energies) are solved. Then, the dissociation rate coefficients have to be parameterized using these temperatures.

The most common multitemperature model is due to Park [1,7,8] (referred to henceforth as Park's model), where the rate coefficients are obtained by computing thermal equilibrium-based dissociation rate coefficients at a modified effective temperature T_e. Park [7,8] used a square-root model, where $T_e = \sqrt{T_t T_v}$. This straightforward model performs reasonably well at high temperatures [7,8,29,30,40,41], and it has been compared to rate coefficients derived from quasi-classical trajectory (QCT) simulations [12,14,19,20,36,42]. However, the model neglects the possibility of rotational nonequilibrium and implicitly assumes that $T_r = T_t$. At lower temperatures, the approximation is reasonable because the vibrational relaxation time scale is significantly longer than rotational relaxation. At high temperatures, though, the rotational relaxation time scale approaches that of vibrational relaxation [17,41,43], thus indicating that $T_r \approx T_v$. As such, the dissociation rate coefficient has also been calculated under the assumption that $T_r \approx T_v$ [26,44]. At moderate temperatures, where rotational relaxation is slow but not the same as vibrational relaxation, T_r should be treated independently, as suggested by Park [41]. Consequently, there is a need to understand the effect of rotational temperature on the dissociation rates.

With this background, the focus of this study is nitrogen dissociation via the following reaction:

$$\mathrm{N}_2(v_1, J_1) + \mathrm{N}_2(v_2, J_2) \rightarrow \mathrm{N}_2(v_3, J_3) + \mathrm{N} + \mathrm{N} \tag{1}$$

For this purpose, the quasi-classical trajectory (QCT) analysis method is used [45–47]. This approach has been used to study other hypersonic-relevant reactions [12,19,22,33,36–38,42], including this reaction [20,26,44]. For instance, regarding the title reaction, with the same potential energy surface (PES) used in this work, Bender et al. [20] calculated the dissociation rate coefficient as a function of $T = T_t = T_r$ and T_v at 25 unique temperature combinations. This work extends the previous studies of the title reaction by treating the rotational temperature independently. The rate coefficient is calculated over a large range of temperature combinations, including low temperatures near the dissociation threshold. To this end, a novel selective sampling procedure is developed that significantly improves the convergence of QCT-calculated rate coefficients, especially at low temperatures. Finally, these results are used to formulate a simple multitemperature rate coefficient expression.

The remainder of this work is organized as follows. Section II describes the selective sampling procedure used in the QCT simulation. First, the conventional Monte Carlo integration formulation of the rate coefficient is presented, followed by the necessary modifications for selective sampling. Section III presents the QCT-calculated dissociation rate coefficients of nitrogen obtained in this work. These results consist of three studies. First, the thermal equilibrium rate coefficient is compared to previous QCT studies to verify the sampling method and to experimental data to validate the rate coefficient calculations. Then, the three-temperature rate coefficient is presented with a focus on how independently choosing T_r modifies the rate coefficient expression. Finally, a three-temperature rate coefficient model, which might be implemented in CFD codes, is presented.

II. Selective Sampling Quasi-Classical Trajectory Formulation

The dissociation rate coefficient is calculated from QCT analysis using Monte Carlo (MC) integration with selective sampling. In addressing this formulation, the following sections describe 1) calculation of the dissociation rate coefficient for a fixed rovibrational state using conventional MC integration theory as implemented in most QCT simulations; 2) modification of the dissociation rate coefficient calculation introduced by selective sampling; and 3) extension of the dissociation rate coefficient calculation so that the rotational and vibrational states are also sampled based on their PDFs.

A. Conventional Dissociation Rate Calculation

Each trajectory is initialized by the phase of the reactants $\boldsymbol{\tau}$, the relative translational speed of the reactants g, and the impact parameter b. Here, $\boldsymbol{\tau}$ describes that initial orientation, vibration phase, and rotation vector for both reactants, which are determined from initial rovibrational quantum numbers $\boldsymbol{n} = (v_1, v_2, J_1, J_2)$. Note that the initial separation of the reactants was set so that the initial force between the reactants was negligible (at least 15 Å for this PES [44]). Because trajectories of the nuclei are treated classically, the outcome of each trajectory is a delta function $\delta_d(g, \boldsymbol{n}, b, \boldsymbol{\tau})$, which represents whether or not the dissociation occurs. The mean probability of dissociation $P_d(g, \boldsymbol{n}, b)$ is defined by integrating over the initial phase of the reactants [48]:

$$P_d(g, \boldsymbol{n}, b) = \int_\tau \delta_d(g, \boldsymbol{n}, b, \boldsymbol{\tau}) f_\tau(\boldsymbol{\tau})\, \mathrm{d}\boldsymbol{\tau} \tag{2}$$

where $f_\tau(\boldsymbol{\tau})\mathrm{d}\boldsymbol{\tau}$ is the PDF, and the corresponding integral is over the full domain. MC integration is used to approximate this integral by tracking the outcomes of many sampled trajectories. Let N denote the number of sampled trajectories for fixed (g, $\boldsymbol{n}$, b) with $\boldsymbol{\tau}$ randomly sampled according to $f_\tau(\boldsymbol{\tau})\mathrm{d}\boldsymbol{\tau}$. Then, Eq. (2) is approximated by [48]

$$P_d(g, \boldsymbol{n}, b) \approx \frac{N_d}{N} \tag{3}$$

where N_d is the number of trajectories resulting in dissociation. In the limit where $N \rightarrow \infty$, the true dissociation probability is attained.

For $N < \infty$, there exists an inherent statistical uncertainty associated with the observed mean. In this work, we define the relative uncertainty ε as two standard deviations normalized by the mean so that $P_d(1 \pm \varepsilon)$ corresponds to the 95% confidence interval of the probability (assuming the sampled mean value is normally distributed). In the figures that follow, we use this interval to denote the uncertainty. Based on the definition of the standard deviation in [46], ε is given by

$$\epsilon = 2\left(\frac{1}{N_d} - \frac{1}{N}\right)^{1/2} \approx \left(\frac{4}{N_d}\right)^{1/2} \tag{4}$$

where the approximation is valid under the assumption that $N_d \ll N$. Thus, for low-probability states, the uncertainty largely depends on the number of dissociative trajectories observed. For example, approximately 400 dissociative trajectories must be observed for a relative uncertainty of $\pm 10\%$ (i.e., $\varepsilon = 0.1$).

The dissociation cross section is calculated by integrating the phase-averaged dissociation probability P_d along the impact parameter weighted by $2\pi b$ [48]:

$$\sigma_d(g, \boldsymbol{n}) = \int_0^{b_{\max}} 2\pi b P_d(g, \boldsymbol{n}, b)\, \mathrm{d}b \tag{5}$$

where $P_d(g, \boldsymbol{n}, b) = 0$ for all $b > b_{\max}$. Like the average dissociation probability, the cross section is approximated by MC integration [48], which reduces Eq. (5) to

$$\sigma_d(g, \boldsymbol{n}) \approx \pi b_{\max}^2 \frac{N_d}{N} \tag{6}$$

where now N refers to trajectories wherein both $\boldsymbol{\tau}$ and b are randomly sampled according to their respective PDFs. The 95% confidence

interval of the dissociation cross section is $\sigma_d(1 \pm \varepsilon)$. That is, the definition of the relative uncertainty of the cross section is equivalent to the relative uncertainty of the probability. The difference is in how trajectories are sampled; b is fixed when calculating the probability, and b is randomly sampled when calculating the cross section.

Finally, the dissociation rate coefficient is defined by integrating the cross section over the relative translational speed weighted by its PDF, i.e.,

$$k_d(\boldsymbol{n}; T_t) = \int_0^\infty g f_g(g; T_t) \sigma_d(g, \boldsymbol{n})\, \mathrm{d}g \tag{7}$$

where $f_g(g; T_t)$ is the Maxwell distribution, given by

$$f_g(g; T_t) = \left(\frac{\mu}{2\pi k_B T_t}\right)^{3/2} 4\pi g^2 e^{-\mu g^2/2k_B T_t} \tag{8}$$

where μ is the reduced mass of the reactants, and k_B is the Boltzmann constant. Similar to the dissociation cross section and probability, MC integration is used to approximate Eq. (7) [48], which becomes

$$k_d(\boldsymbol{n}; T_t) \approx \pi b_{\max}^2 \left(\frac{8k_B T_t}{\pi\mu}\right)^{1/2} \frac{N_d}{N} \tag{9}$$

where now N refers to trajectories wherein $\boldsymbol{\tau}$, b, and g are randomly sampled according to their respective PDFs. As before, the 95% confidence interval of the dissociation rate is $k_d(1 \pm \varepsilon)$, where ε is defined in Eq. (4). Consider a few final remarks regarding Eq. (9). First, $k_d(\boldsymbol{n}; T_t)$ is extended to $k_d(T_t, T_r, T_v)$ by sampling the rotational and vibrational quantum numbers from their respective PDFs. Second, because both the reactants are identical for the reaction considered in this work, both "double-counting" and "double-dissociation" events are accounted using the same approach presented by Bender et al. [20]. That is, the double-dissociation rate coefficient is calculated, multiplied by 2, and then added to the calculated single-dissociation rate coefficient. Then, this combined rate coefficient is divided by 2 to account for double-counting.

B. Selective Sampling the Relative Translational Speed

Selective sampling is now employed so that only trajectories with sufficient energy to cause dissociation are sampled. Note that the approximation of the cross section still follows the conventional sampling technique employed in most QCT simulations because the initial phase and the impact parameter do not directly determine a probability of reaction per trajectory a priori. However, without affecting the rate calculation, the lower bound of the integral in Eq. (7) can be increased to a minimum relative speed necessary for dissociation, denoted g_o. We enforce the condition that the first reactant's center of mass is stationary, and so the minimum initial speed of the second reactant is defined as

$$g_o(\boldsymbol{n}) = \left(\frac{2}{M_2}(E_d - E_{rv}(\boldsymbol{n}))\right)^{1/2} \tag{10}$$

where E_{rv} is total rovibrational energy of both reactants, and M_2 is the total mass of the second reactant. For high-lying rovibrational states wherein $E_d - E_{rv}(\boldsymbol{n}) < 0$, this indicates that the rovibrational energy is sufficient for dissociation, and g_o is set to zero. In short, $\delta_d(g, \boldsymbol{n}, b, \boldsymbol{\tau}) = 0$ for all $g < g_o(\boldsymbol{n})$, and so Eq. (7) is equivalently defined as

$$k_d(\boldsymbol{n}; T_t) = \int_{g_o(n)}^\infty g f_g(g; T_t) \sigma_d(g, \boldsymbol{n})\, \mathrm{d}g \tag{11}$$

To approximate this integral using Monte Carlo sampling, first define a new variable g' such that

$$C\mathrm{d}g' = g f_g(g; T_t)\, \mathrm{d}g \tag{12}$$

where C is a function independent of relative speed that is to be determined. After integrating this equation, two requirements are imposed on g' to calculate C: 1) when $g = g_o(\boldsymbol{n})$, $g' = 0$; and 2) when $g = \infty$, $g' = 1$. Based on these constraints,

$$C = \left(\frac{8k_B T_t}{\pi\mu}\right)^{1/2} \left(1 + \frac{\mu g_o(n)^2}{2k_B T_t}\right) e^{-\mu g_o(\boldsymbol{n})^2/2k_B T_t} \tag{13}$$

and

$$g' = 1 - \exp\left(\frac{-\mu(g^2 - g_o(\boldsymbol{n})^2)}{2k_B T_t}\right)\left(\frac{1 + \mu g^2/2k_B T_t}{1 + \mu g_o(\boldsymbol{n})^2/2k_B T_t}\right) \tag{14}$$

both of which are functions of T_t and $\boldsymbol{n}$. We define the minimum speed factor $\xi(\boldsymbol{n}; T_t)$ as the factor introduced when using this sampling procedure, i.e.,

$$\xi(\boldsymbol{n}; T_t) = \left(1 + \frac{\mu g_o(n)^2}{2k_B T_t}\right) e^{-\mu g_o(\boldsymbol{n})^2/2k_B T_t} \tag{15}$$

This factor is defined such that $\xi = 1$ if $g_o = 0$. Now, Eq. (11) is given by

$$k_d(\boldsymbol{n}; T_t) = \xi(\boldsymbol{n}; T_t) \left(\frac{8k_B T_t}{\pi\mu}\right)^{1/2} \int_0^1 \sigma_d(g(g'), \boldsymbol{n})\, \mathrm{d}g' \tag{16}$$

Incorporating Eq. (6), Eq. (16) is approximated as

$$k_d(\boldsymbol{n}; T_t) \approx \pi b_{\max}^2 \xi(\boldsymbol{n}; T_t) \left(\frac{8k_B T_t}{\pi\mu}\right)^{1/2} \frac{N_d}{N} \tag{17}$$

where now N refers to trajectories wherein $\boldsymbol{\tau}$, b, and g are randomly sampled according to their respective PDFs. For the speed, this corresponds to sampling g' uniformly from 0 to 1 and solving Eq. (14) iteratively. Note that selective sampling does not alter the definition of the relative uncertainty as defined in Eq. (4).

C. Selectively Sampling the Rovibrational Quantum Numbers

To this point, the rate coefficient has been defined for a specific initial rovibrational state. Now, it is assumed that the rotational and vibrational states of the reactants are described by Boltzmann distributions characterized by T_r and T_v, respectively. As with the relative speed, the sampling procedure is modified so that one only simulates trajectories in which the initial energy of the system has sufficient energy to cause dissociation. To start, the state-specific dissociation rate coefficient is averaged over the rovibrational states so that

$$k_d(T_t, T_r, T_v) = \sum_n f_{rv}(\boldsymbol{n}; T_r, T_v) k_d(\boldsymbol{n}; T_t) \tag{18}$$

where the summation is over the full set of initial quantum states, and $f_{rv}(\boldsymbol{n}; T_r, T_v)$ is the initial rovibrational state PDF of both reactants and is defined in the Appendix. Now, substituting Eq. (16) into Eq. (18) and rearranging, we obtain

$$k_d(T_t, T_r, T_v) = \left(\frac{8k_B T_t}{\pi\mu}\right)^{1/2} \times \sum_n \left(f_{rv}(\boldsymbol{n}; T_r, T_v)\xi(\boldsymbol{n}; T_t) \int_0^1 \sigma(g(g'), \boldsymbol{n})\, \mathrm{d}g'\right) \tag{19}$$

Because the factor $\xi(\boldsymbol{n}; T_t)$ is a function of the initial rovibrational state, the sampling procedure must be modified. We define the effective PDF of the initial rovibrational states:

$$f'_{rv}(\boldsymbol{n}; T_t, T_r, T_v) = \frac{f_{rv}(\boldsymbol{n}; T_r, T_v)\xi(\boldsymbol{n}; T_t)}{Q'_{rv}(T_t, T_r, T_v)} \tag{20}$$

where Q'_{rv} is the effective partition function given by

$$Q'_{rv}(T_t, T_r, T_v) = \sum_n f_{rv}(\boldsymbol{n}; T_r, T_v)\xi(\boldsymbol{n}; T_t) \tag{21}$$

With this definition, Eq. (19) becomes

$$k_d(T_t, T_r, T_v) = \left(\frac{8k_B T_t}{\pi\mu}\right)^{1/2} Q'_{rv}(T_t, T_r, T_v) \times \sum_n f'_{rv}(\boldsymbol{n}; T_t, T_r, T_v) \int_0^1 \sigma(g(g'), \boldsymbol{n})\, \mathrm{d}g' \tag{22}$$

Noting that f'_{rv} is unit-normalized, $\boldsymbol{n}$ can be randomly sampled from f'_{rv} to approximate the summation. With the MC approximation of the integral, Eq. (22) is reduced to

$$k_d(T_t, T_r, T_v) \approx \pi b_{\max}^2 Q'_{rv}(T_t, T_r, T_v)\left(\frac{8k_B T_t}{\pi\mu}\right)^{1/2} \frac{N_d}{N} \tag{23}$$

where now N refers to trajectories wherein $\boldsymbol{\tau}$, b, g, and $\boldsymbol{n}$ are all randomly sampled according to their corresponding PDFs. This is the Monte Carlo approximation of the dissociation rate coefficient with selective sampling. Similar to before, if $g_o = 0$, then $Q'_{rv} = 1$, and Eq. (23) is equivalent to Eq. (9). The relative uncertainty is unaltered from its original definition, and so the 95% confidence interval of the rate coefficient is still $k_d(1 \pm \varepsilon)$, where ε is defined in Eq. (4).

It is useful to combine Q'_{rv} and N to understand how selective sampling modifies Eq. (23) compared the conventional sampling procedure. To this end, we define the effective number of trajectories N_{eff} by

$$N_{\text{eff}}(T_t, T_r, T_v) = N/Q'_{rv}(T_t, T_r, T_v) \tag{24}$$

Now, Eq. (23) becomes

$$k_d(T_t, T_r, T_v) \approx \pi b_{\max}^2 \left(\frac{8k_B T_t}{\pi\mu}\right)^{1/2} \frac{N_d}{N_{\text{eff}}} \tag{25}$$

which is the equivalent to the definition of the rate coefficient defined with conventional sampling [see Eq. (9)]. In summary, by selectively sampling the relative speed, we are effectively increasing the number of trajectories by $1/Q'_{rv}$ compared to the actual number of simulated trajectories. Consider then that N_{eff} defines the theoretical number of conventionally sampled trajectories required to match the uncertainty compared to selectively sampled trajectories.

III. Results

Using the selective sampling technique, the dissociation rate coefficient of nitrogen was calculated using an in-house QCT program optimized for message passing interface (MPI)-based parallel simulations on high-performance computing clusters. Details are presented in [26,42]. The numerical ODE solver was the adaptive Runge–Kutta Prince–Dormand method [49] as implemented in the open-source GNU Scientific Library. This method is not symplectic, but the error tolerance was set sufficiently low so that the total energy of the system did not drift significantly along a trajectory relative to the uncertainty in the PES. The analytical PES used in this work was developed by Bender et al. [50], which was an extension of the surface developed by Paukku et al. from a set of approximately 17,000 ab initio data points [51]. The maximum impact parameter was set as 6 Å based on previous studies using this PES [20,26]. To define the initial state, first the rovibrational is sampled from f'_{rv} for a given T_t, T_r, and T_v, as defined in Eq. (20). Then, the lower bound of the relative speed is determined using Eq. (10), and the relative speed was sampled from the modified PDF as presented in Sec. II.B.

Before the QCT simulation, the reaction barrier of the PES was calculated. To this end, trajectories were randomly simulated until a dissociative trajectory was observed. Then, this reactive trajectory's path was adjusted using the nudged elastic band method until it followed a minimum-energy path [52,53]. The reaction barrier (i.e., the dissociation energy E_d) was defined as the maximum energy of this path. It was found that the reaction energy barrier was approximately 230 kcal/mol. This process was repeated several times to ensure that the observed minimum energy was consistent. To be conservative, E_d was set to 220 kcal/mol.

In total, 729 (i.e., 9^3) unique rate coefficients were directly calculated, with T_t, T_r, and T_v each sampled at 6000, 8000, 10,000, 13,000, 20,000, 30,000, 40,000, 50,000, and 60,000 K. Trajectories were simulated on the Texas Advanced Computing Center computing clusters on approximately 4000 cores over the course of 40 h. A total of 5.35 billion trajectories were directly simulated, which will be shown to correspond to 53.9 billion effective trajectories as defined in Eq. (24). The set of directly calculated rate coefficients was then projected onto a dense grid of temperatures using the interpolation scheme presented by Wang et al. [54] as implemented in [26,42]. The temperature increment of the interpolated set was 1000 K, resulting in 166,375 (i.e., 55^3) total rate coefficients, which is dense enough to be directly imported into CFD programs.

In the following discussion, 1) the effective trajectories from selective sampling are discussed with regard to nitrogen dissociation; 2) the thermal equilibrium rate coefficient (i.e., $T_t = T_r = T_v$) is compared to previous QCT studies and experimental data to verify and validate the results; 3) the nonequilibrium rate coefficient is analyzed with a focus on how independently choosing T_r modifies the rate coefficient expression; and 4) a new three-temperature reaction rate coefficient model is presented and compared to previous studies.

A. Effective Trajectories for Nitrogen Dissociation

The ratio N_{eff}/N is a measure of the computational benefit achieved by selectively sampling trajectories at a specified temperature. For the title reaction, Fig. 1 shows the ratio evaluated

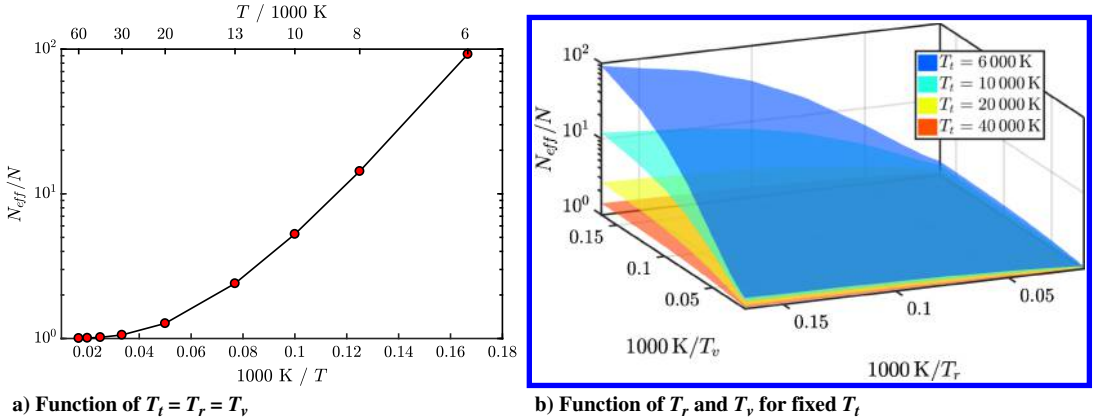

a) Function of $T_t = T_r = T_v$ **b) Function of T_r and T_v for fixed T_t**

Fig. 1 Ratio of effective number of trajectories compared to sampled trajectories at different temperatures.

at the sampled temperatures, including the ratio when $T_t = T_r = T_v$ and the ratio as a function of T_r and T_v for fixed T_t.

At and below 8000 K, the effective number of trajectories simulated is at least an order of magnitude greater than the actual number of trajectories simulated. Thus, for a fixed uncertainty at 6000 K, nearly 100 times more trajectories would be needed when using conventional sampling as opposed to the new selective sampling procedure. At higher temperatures, the ratio approaches unity, though it is still significant below 30,000 K. For instance, even for 20,000 K, the ratio represents a 27% increase in the effective number of simulated trajectories, a substantial improvement. Figure 1b shows a wide range of effective trajectory ratios, and the general trends are the same as the set of ratio at thermal equilibrium. As either T_t, T_v, or T_r increases, the ratio is diminished. Interestingly, the ratio is approximately symmetric along the $T_r = T_v$ diagonal. In short, changes in either temperature make similar modifications to the minimum initial speed $g_o(\boldsymbol{n})$ as averaged along the rovibrational PDF, as shown in Eq. (21).

Two observations from this figure are important to discuss. First, note that the inverse of the ratio corresponds to the fraction of conventionally sampled trajectories that have sufficient total energy to dissociate. Thus, at 6000 K, only 1.1% of the conventionally sampled trajectories may result in dissociation, whereas for 20,000 K, 78.6% may result in dissociation. At low temperatures, the necessary energy for dissociation is in the tails of the initial energy distributions, and so the conventional sampling strategy is highly inefficient. Uniform sampling over a wide domain of energies will ensure that the tails are sufficiently sampled, but doing so will also increase the uncertainty of the dissociation rate [42]. Second, for rate coefficients calculated using conventional sampling, the minimum observable dissociation probability corresponds to the inverse of the number of trajectories simulated (i.e., $1/N$). However, using the selective sampling technique, the minimum probability is the inverse of the effective number of trajectories (i.e., $1/N_{\text{eff}}$). Thus, for 10 million selectively sampled trajectories at 6000 K, the minimum resolution of the dissociation probability is reduced from 10^{-7} to approximately 10^{-9}. This improvement in accuracy is critical in determining the reaction rate coefficient at low temperatures.

B. Verification and Validation of Selective Sampling Technique

The selective sampling technique was verified by comparing the thermal equilibrium dissociation rate coefficient $k_d^{\text{eq}}(T)$ to those calculated by Bender et al. [20], which were calculated using the same PES. Below 13,000 K, the rate coefficients were also compared to experimental data as a means of validation [55,56]. Here, the temperature range of the QCT results ranged from 6000 to 60,000 K. Table 1 summarizes the results.

A total of 236 million trajectories were directly simulated at these temperatures, which corresponded to 13.1 billion effective trajectories. Note that approximately 93% of the effective trajectories are for the rate coefficient at 6000 K. The relative uncertainty ranged from 0.1 to 11% of the calculated values. Note that selective sampling does not imply a constant convergence. For instance, at 20,000 and 30,000 K, the relative uncertainty is approximately the same, but at 20,000 K, approximately 4.2 million more trajectories were required.

Table 1 Thermal equilibrium dissociation rate coefficient using selective sampling

T, K	N_d	N	N_{eff}	k_d^{eq}, cm^3/(mol · s)	ε
6,000	345	1.320×10^8	1.218×10^{10}	2.905×10^7	1.077×10^{-1}
8,000	1,600	4.982×10^7	7.136×10^8	2.655×10^9	5.000×10^{-2}
10,000	3,946	2.208×10^7	1.163×10^8	4.494×10^{10}	3.183×10^{-2}
13,000	19,672	2.207×10^7	5.300×10^7	5.604×10^{11}	1.426×10^{-2}
20,000	40,404	5.960×10^6	7.582×10^6	9.979×10^{12}	9.923×10^{-3}
30,000	40,918	1.738×10^6	1.839×10^6	5.103×10^{13}	9.777×10^{-3}
40,000	41,224	9.700×10^5	9.887×10^5	1.104×10^{14}	9.643×10^{-3}
50,000	41,978	7.240×10^5	7.301×10^5	1.702×10^{14}	9.477×10^{-3}
60,000	43,101	6.020×10^5	6.047×10^5	2.312×10^{14}	9.284×10^{-3}

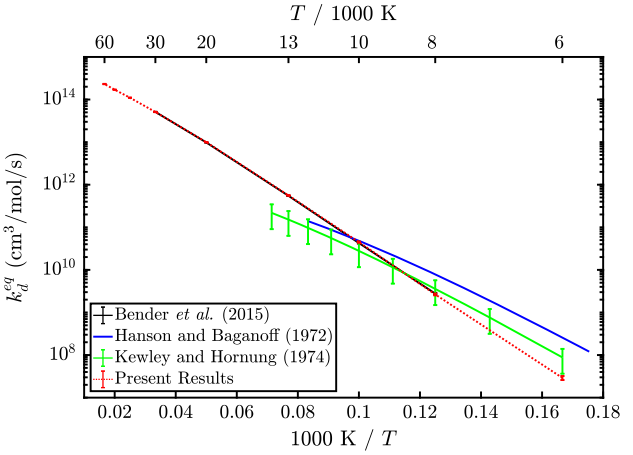

Fig. 2 Thermal equilibrium dissociation rate coefficient using selective sampling.

Figure 2 shows the presently calculated results compared to with previous studies (plotted over their corresponding valid domains).

The present results closely match the rate coefficients presented by Bender et al. [20], which were calculated between 8000 and 30,000 K. All of the rate coefficients are within the uncertainty bounds. In summary, we feel that this is a strong verification of the selective sampling method.

As validation of both the PES and the QCT method, we compare our calculated rate coefficients along the full range of experimentally derived rate coefficient expressions by Hanson and Baganoff [55] and Kewley and Hornung [56]. The present results were used to generate a standard Arrhenius rate expression using a nonlinear least-squares fitting method. The resulting expression is given by

$$k_d^{\text{eq}}(T) \approx (4.325 \pm 0.122) \times 10^{17} T^{-0.519} \exp\left(-\frac{1.132 \times 10^5}{T}\right) \text{cm}^3/(\text{mol} \cdot \text{s}) \quad (26)$$

where the variance in leading coefficient was determined based on the upper and lower bounds of the calculated rate coefficient [i.e., $k_d(1 \pm \varepsilon)$], as shown in Fig. 2. Compared to the experimentally derived values, the QCT-calculated results have a stronger dependence on temperature. At 6000 K, the present results slightly underpredict the rate coefficient; from 8000 to 10,000 K, there is good agreement with the experimental data; and above 10,000 K, the rate coefficient is significantly overpredicted. For instance, at 13,000 K, the QCT-calculated rate coefficient is approximately 3.7 times greater than the experimental value presented by Kewley and Hornung [56]. From 8000 to 10,000 K, there is good agreement with the experimental data.

There are several possible reasons for the discrepancy between the experimental and calculated rate coefficients, and more studies are necessary to resolve this question. We examine three possible sources of error. First, consider the classical assumption of the QCT method. At low temperatures (less than 1000 K) and for light molecules (e.g., H_2), the classical assumption is known to neglect important tunneling effects. However, for the N_2 dissociation at the conditions of interest, the temperatures are high and the reactants heavy, and so the classical assumption is likely valid, and we do not believe that this is a significant source of error. Second, the PES may not be accurate enough, even though it represents the state of the art and was developed for QCT simulations in this temperature range [20,51]. The PES has been modified once before to improve long-range interactions [20], and other improvements may also help improve agreement with experiments. Finally, the rate coefficients derived from shock-tube experiments are based on the assumption of complete thermal equilibration during the induction period, before the beginning of dissociation. This is unlikely to be true especially at very high temperatures where high-lying (and more readily dissociated) vibrational states are likely to be underpopulated during

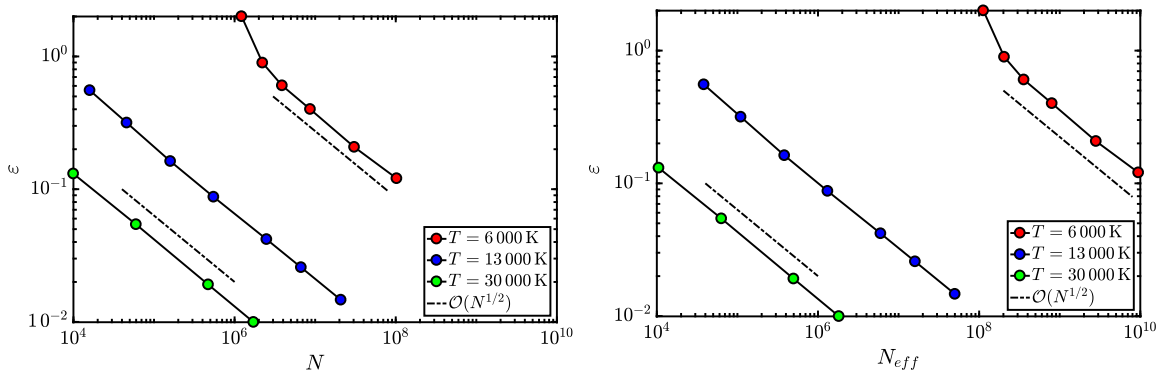

a) Versus simulated trajectories **b) Versus effective trajectories**

Fig. 3 Convergence of the relative uncertainty of the dissociation rate coefficient.

much of the experimental measurement. Master equation simulations have shown that the vibrational population distribution evolves to a steady-state nonequilibrium distribution after shock heating. For example, Gonzales and Varghese [57] show that, for N_2 dilute in Ar shock heated to 10,000 K, the steady-state dissociation rate is about 10% of the thermal equilibrium rate. A Boltzmann distribution of vibrational states at the final temperature is only attained via recombination of atoms into the highest-lying vibrational states [58]. The thermal equilibrium rates computed here are obtained by imposing equilibrium rovibrational distributions when computing weighted sums of the state-specific rates. State-specific master equation simulations of the shock tube measurements are needed to determine what rates would be observed in the experiments.

The convergence of the rate coefficient was also analyzed by calculating ε at "checkpoints" throughout the full QCT simulation. Figure 3a show ε versus the number of simulated trajectories at 6000, 13,000, and 30,000 K.

The convergence rate (i.e., the slope of the curves) is $\mathcal{O}(N^{1/2})$, which is expected for Monte Carlo integration. Figure 3b shows the same curves now plotted as a function of the effective trajectories; this serves as an indication of the expected convergence if conventional sampling were used. In comparing the two figures, we conclude that selective sampling does not improve the convergence rate of ε, but instead it shifts the curves so that fewer trajectories are necessary. At high temperatures, this shift is marginal, but at low temperatures, the shift shows that selective sampling offers a significant advantage.

In summary, the selective sampling technique was verified and validated using previous studies. It was also observed that the required number of simulated trajectories for a given relative tolerance was significantly decreased, especially at low temperatures.

C. Nonequilibrium Dissociation Rate

With selective sampling verified and validated for thermal equilibrium, the nonequilibrium rate coefficient was calculated as a function of independently defined T_t, T_r, and T_v. The directly calculated rate coefficients were then interpolated to calculate the rate coefficient at 1000 K intervals using the scheme presented by Wang et al. [54], as implemented in [26,42]. Similar to the rate coefficients calculated at thermal equilibrium, the nonequilibrium results were compared to those presented by Bender et al. [20] (calculated assuming $T_r = T_t$ between 8000 and 30,000 K), as shown in Fig. 4.

The circle symbols at 30,000 K denote rate coefficients wherein the coefficients are not within the uncertainty bounds of one another. This occurs at three temperature combinations, each of which are characterized by high T and low T_v. Overall, though, both sets of data match closely, and all of the presently calculated results are within approximately 5% of the rate coefficients presented by Bender et al. [20].

To visualize the three-temperature nonequilibrium rate coefficient, it is convenient to examine the rate in two dimensions along slices. Here, T_r is set as T_t, $(T_t + T_v)/2$, and T_v, and the rate coefficient is plotted as a function of T_t and T_v, as shown in Fig. 5.

The different ways of defining T_r relative to T_t and T_v show the subtle influence that rotational temperature has on the dissociation

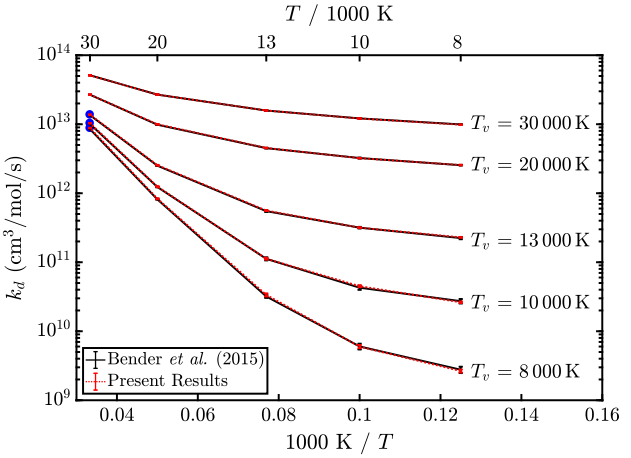

Fig. 4 Thermal nonequilibrium dissociation rate coefficients compared with Bender et al. [20].

rate of nitrogen. For $T_r = T_t$ in Fig. 5a, the rate coefficient is approximately symmetric along the diagonal for low T_t and T_v, which implies that both T_t and T_v equally influence the rate coefficient. However, this symmetry is lost as T_t and T_v increase, with changes in T_t now having a more significant impact on the rate coefficient than T_v. This is because as T_t increases, so too does T_r, which impacts the rate coefficient more significantly than just increasing T_v.

Similar observations can be made in Figs. 5b and 5c. For $T_r = T_v$ (Fig. 5c), symmetry is observed at high T_t and T_v, but the rate coefficient is skewed for low T_t and T_v. Here, changes in T_v will have a more significant impact on the rate coefficient compared to T_t, which is the opposite effect observed in Fig. 5a. The trends from Figs. 5a and 5c are both present when T_r is averaged between T_t and T_v, as shown in Fig. 5b. Here, the rate coefficient is only symmetric along the diagonal for moderate T_t and T_v. Overall, these observations are similar to those presented in previous work by Voelkel et al. [26] and Bender et al. [20,44]. However, the dependence of the rate coefficient on T_r independent of T_t and T_v is unique to this work and necessary in deriving a three-temperature rate coefficient model (see Sec. III.D for more details).

The present results are compared to Park's two-temperature model [7], which assumes that $T_r = T_t$ and $k_d(T_t, T_v) = k_d^{\text{eq}}(\sqrt{T_t T_v})$, as shown in Fig. 6 ($k_d^P$ is used to denote Park's model).

Park's model is symmetric along the diagonal for all temperatures. This contrasts the QCT-calculated rate coefficients, which become skewed at high temperatures (see Fig. 5a). Furthermore, the nature of the curvature at low temperatures is dissimilar to the QCT-calculated rate coefficient. These differences are observed in Fig. 6b, which shows the relative difference between Park's model and the QCT results on a log scale. The figure shows that Park's model is only valid at high temperatures and when T_v is close to T_t. It was observed that,

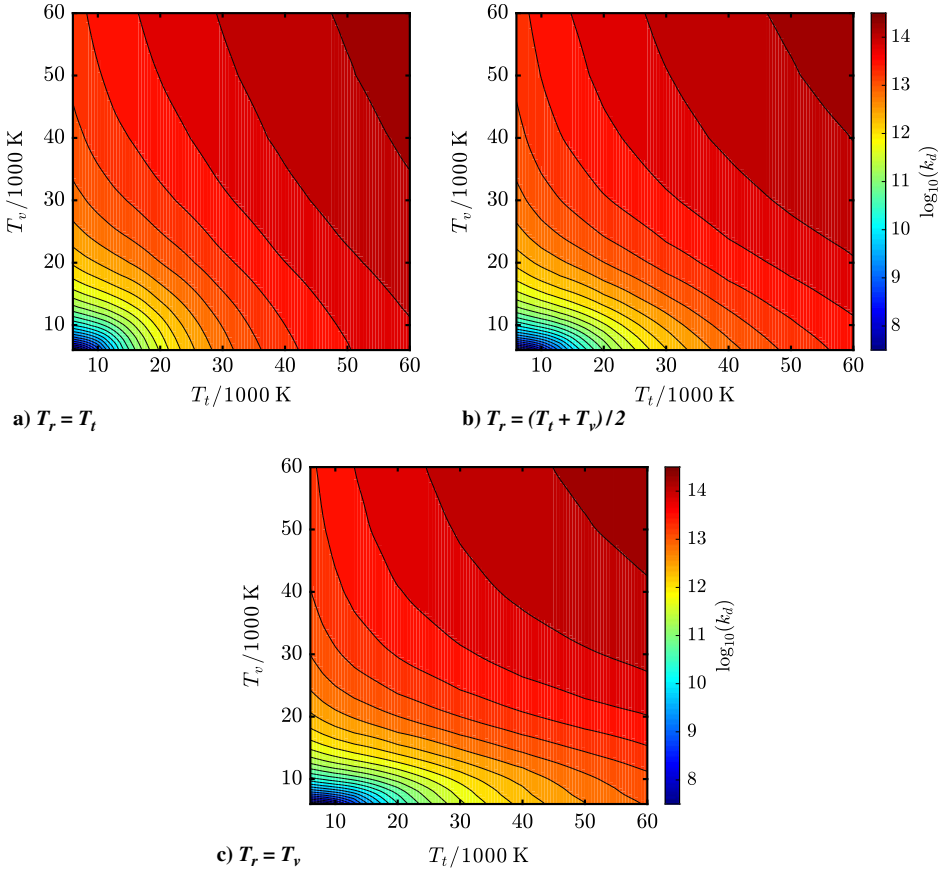

Fig. 5 Nonequilibrium dissociation rate coefficient (units of k_d are cubic centimeters per mole per second).

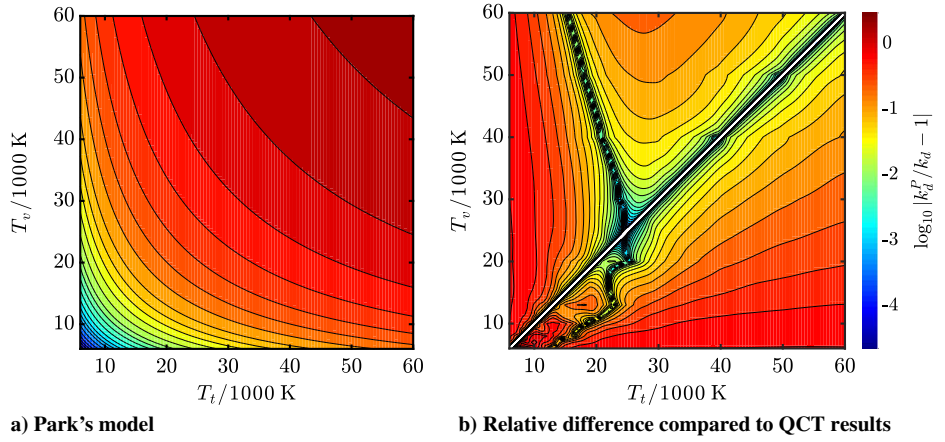

Fig. 6 Nonequilibrium rate coefficient via Park's model and the relative difference compared to QCT-calculated rate coefficients (units of k_d are cubic centimeters per mole per second).

when $T_t > 20{,}000$ K and $0.7 \leq T_v/T_t \leq 1.5$, Park's model was within approximately 10% of the QCT results (i.e., $\log_{10}|k_d^P/k_d - 1| \leq 0.1$ in Fig. 6b). In summary, Park's model is only applicable in this subdomain, and the model does not accurately predict the shift in the rate coefficient's sensitivity toward T_t.

The relative uncertainty of the directly calculated rate coefficients is visualized similarly and shown in Fig. 7. Note that this figure only shows the uncertainty of the rate coefficients directly calculated in the QCT simulation and that other temperature combinations showed similar results.

At moderate and high temperatures, the relative uncertainty is approximately 1%. This was the desired tolerance of the QCT simulation, and so trajectories were no longer simulated once the tolerance was achieved. At low temperatures, the uncertainty is higher, reaching a maximum value of approximately 18% uncertainty. Rate coefficients for low T_v resulted in a higher uncertainties compared to low T_t. This is due to the fact that higher relative speeds are sampled to account for the low rovibrational energy, which gives the reactants less time to interact. That said, the number of simulated trajectories per temperature combination varied considerably depending on the frequency at which dissociation trajectories were observed. Figure 8 shows the number of trajectories simulated and the corresponding effective number of trajectories along the slice where $T_r = (T_t + T_v)/2$.

For high temperatures, only approximately 1 million trajectories were required to obtain the 1% relative uncertainty limit (see Fig. 7 for reference). At the low temperatures, approximately 130 million trajectories were simulated per temperature combination. Referenc-

ing Fig. 8a, this corresponds to a tremendous number of effective trajectories. For example, $N_{\text{eff}} \approx 12$ billion when $T_t = T_v = 6000$ K (more than double the number of total simulated trajectories in this work). This clearly demonstrates the advantage of selective sampling compared to the conventional method for accurately calculating the dissociation rate coefficients at lower temperatures.

D. Three-Temperature Rate Coefficient Model

The QCT-calculated dissociation rate coefficients were projected onto a functional form dependent on T_t, T_r, and T_v. This model is derived from the following observation: given a nonequilibrium rate coefficient at a given T_t, T_r, and T_v, there exists a unique effective temperature T_e such that

$$k_d(T_t, T_r, T_v) = k_d^{\text{eq}}(T_e) \tag{27}$$

However, the determination of T_e is nontrivial. Here, it is defined similar to the form originally proposed by Park [7]:

$$T_e = T_t^{c_1} T_r^{c_2} T_v^{c_3} \tag{28}$$

where $c_1 + c_2 + c_3 = 1$ is enforced. The accuracy of the model was quantified using the rms of the relative error of the fit, i.e.,

$$\left\| \frac{k_d^{\text{eq}}(T_e) - k_d(T_t, T_r, T_v)}{k_d(T_t, T_r, T_v)} \right\|_2 \tag{29}$$

From the set of calculated dissociation rate coefficients, the coefficients c_1, c_2, and c_3 were calculated for each model using nonlinear least squares. Three fits were determined over differing temperature ranges: 6000 to 60,000 K, 13,000 to 40,000 K, and 30,000 to 60,000 K. The coefficients and the corresponding error of the fit are shown in Table 2.

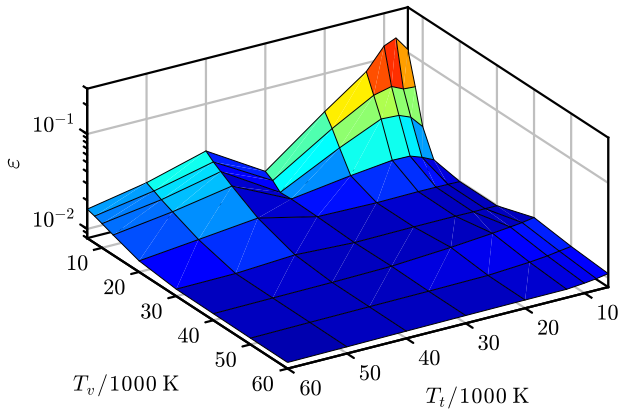

Fig. 7 Relative uncertainty of the nonequilibrium reaction rate coefficient for $T_r = (T_t + T_v)/2$.

Table 2 Coefficients for effective temperature model over varied temperature ranges

Temperature range, K	c_1	c_2	c_3	RMS of error, %
6000–60,000	0.3438	0.2639	0.3923	35.3
13,000–40,000	0.3106	0.2256	0.4638	14.3
30,000–60,000	0.4702	0.1758	0.3540	2.19

The rms error associated with the full domain of temperatures suggests that this fit is a poor representation of the dissociation rate. That is, the "effective temperature" model defined by Eq. (28) does not accurately represent the nonequilibrium rate coefficient over such a wide temperature range. The rapid dropoff of the dissociation rate coefficient at low temperatures contributes significantly to the error.

The fit over the subset of temperatures between 13,000 and 40,000 K shows more promising results, and the rms error is within 14% of the original data. This subset of temperatures was determined to represent the range where the three-temperature model is critical. At lower temperatures, rotational relaxation is fast relative to vibrational relaxation (i.e., $T_r \approx T_t$), and at higher temperatures, rotational and vibrational relaxation rate coefficients are approximately the same (i.e., $T_r \approx T_v$) [17,41,43]. In examining the coefficients of the fit, c_3 is the largest value, which indicates that T_e varies more with T_v compared to T_r and T_t. In other words, the rate coefficient is most sensitive to the vibrational temperature. The fit is compared to the directly calculated rate coefficients along slices, as shown in Fig. 9. Note that the error bars for the directly calculated rate coefficients were small compared to the error of the fits.

Depending on how T_v and T_r are defined, the fit is appears more or less accurate though global patterns are not obvious. For instance, at $T_v = 13{,}000$ K, the QCT calculated rate coefficient is more nonlinear compared to higher T_v, but this behavior is not observed by the model. For $T_r = T_t$ in Fig. 9a, Park's model is also plotted, which closely matches the new model. Consider that Park's model defines $T_e = T_t^{0.5} T_v^{0.5}$ [7], and the new model suggests $T_e = T_t^{0.536} T_v^{0.464}$. The two models are similar, though the new model suggests that the rate coefficient is slightly more sensitive to T_t. For $T_r = T_v$, the slices in Fig. 9b suggest that the data is well represented by the fit. Overall, we conclude that this model performs reasonably well over this wide temperature range.

Finally, we consider the subset of high temperatures ranging from 30,000 to 60,000 K (see Table 2). At these high temperatures, the rate coefficient is approximately log-linear with the inverse of the temperature, which results in a very accurate fit as suggested by the rms error, which less than 3%. Here, the coefficients now suggest that T_t is the dominant mode in determining the effective temperature. As before, slices comparing the model and directly calculated rate coefficients are plotted in Fig. 10.

For $T_r = T_t$ in Fig. 10a, the new model closely matches the data, but Park's model does not. Using the data from Table 2, when $T_r = T_t$, the coefficients result in $T_e = T_t^{0.646} T_v^{0.354}$, which is a significant departure from Park's model (i.e., $T_e = T_t^{0.5} T_v^{0.5}$). However, for high temperatures, it is more likely that $T_r \approx T_v$

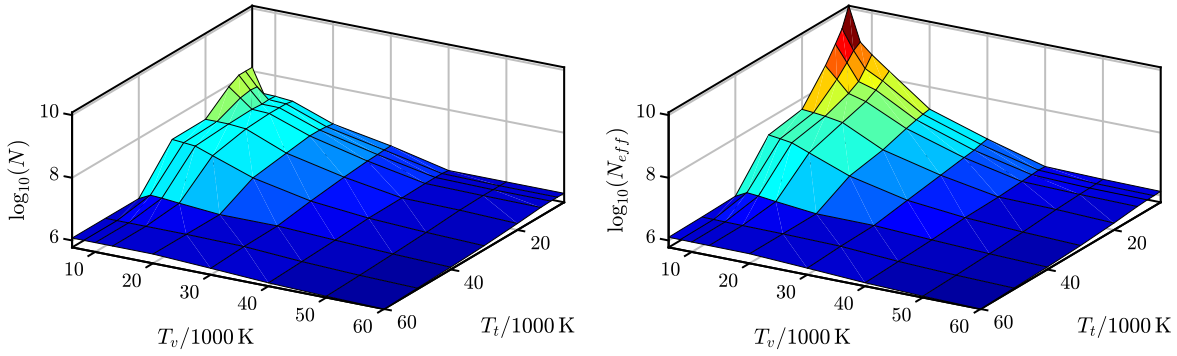

a) Simulated trajectories **b) Effective trajectories**

Fig. 8 Simulated and effective trajectories for $T_r = (T + T_v)/2$.

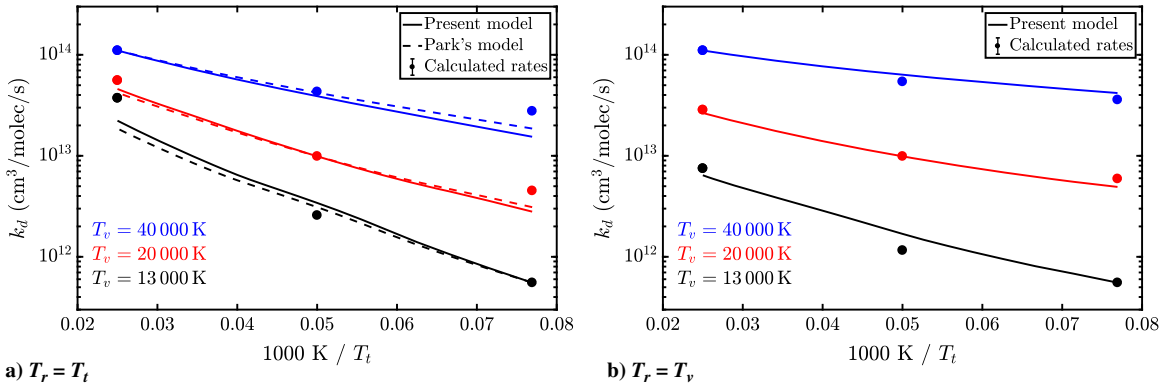

a) $T_r = T_t$ **b)** $T_r = T_v$

Fig. 9 Modeled dissociation rate coefficient along slices for fixed T_v for temperatures ranging from 13,000 to 40,000 K.

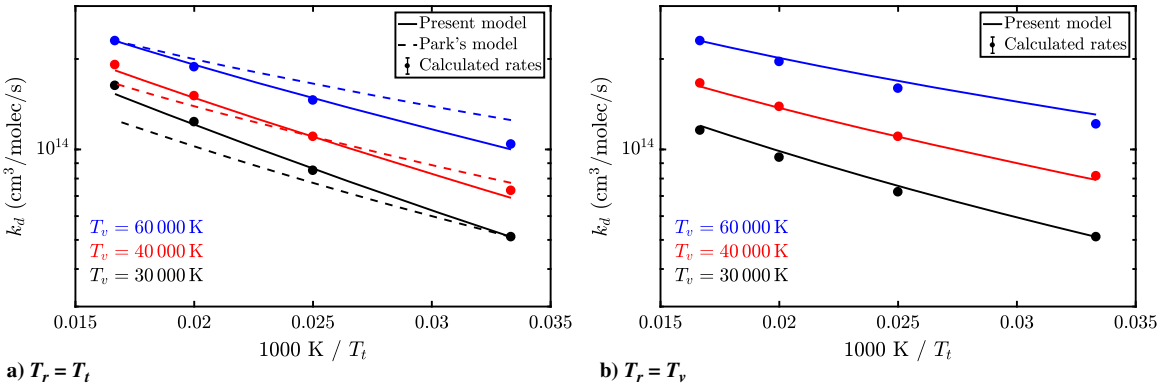

a) $T_r = T_t$ **b)** $T_r = T_v$

Fig. 10 Modeled dissociation rate coefficient along slices for fixed T_v for temperatures ranging from 30,000 to 60,000 K.

because rotational and vibrational relaxation time scales are approximately the same. The three-temperature model predicts the rate coefficient under this condition as well, as shown in Fig. 10b. The model overpredicts the rate coefficient when T_v is low and T_t is high (or vice versa), but these differences are small relative to the rate itself. Overall, between 30,000 and 60,000 K, the effective temperature model is highly accurate, and it can be confidently used in CFD applications for any T_t–T_r–T_v combination.

IV. Conclusions

The dissociation rate of nitrogen was calculated as a function of T_t, T_r, and T_v via quasi-classical trajectory (QCT) analysis. A total of 729 (i.e., 9^3) rate coefficients were directly calculated for temperatures ranging from 6000 to 60,000 K. Previously, calculating this set of rate coefficients using conventional Monte Carlo sampling would have incurred a very large computational burden due to the number of trajectories required to accurately determine the rate coefficient at low temperatures. A novel selective sampling procedure was presented, which only samples trajectories with sufficient energy to cause dissociation. This procedure reduced computational expense considerably, and the uncertainty of the calculated rate coefficients was significantly reduced at low temperatures compared to the conventional sampling method for a fixed number of simulated trajectories.

The selective sampling method was verified by comparing the nonequilibrium rate coefficient with previous QCT calculations by Bender et al. [20], where T_r was assumed to be equal to T_t. The comparisons show at most a 5% difference between the two sets of data, thus verifying the selective sampling procedure. Also, the thermal equilibrium rate coefficient was validated against experimental data from 6000 to 12,000 K. Below 10,000 K, the QCT-calculated rate coefficients are within the uncertainty bounds of the experimental data, but at higher temperatures, the calculated rate coefficient overpredicts dissociation. However, because of the relatively large variance of the experimental data, the authors feel that this sufficiently validates the rate coeffcieint calculations.

From the full set of nonequilibrium rate coefficients, the relative effect of shifting T_r between T_t and T_v was analyzed. The dissociation rate where $T_r = T_t$ and $T_r = T_v$ showed expected results based on previous QCT and experimental nonequilibrium studies. However, this marks the first QCT study of this reaction wherein T_r is treated as an independent variable. By doing so, this could be applied in a computational fluid dynamics (CFD) simulation under several conditions. First, a new transport equation could be added to the governing equations similar to vibrational energy transport. This is a more rigorous model than the conventional two-temperature models that assumes $T_r = T_t$. As a second implementation, the conventional two-temperature model could be extended so that the T_r is approximated based on the local values of T_t and T_v. For instance, at low temperatures, T_r is approximately T_t; at high temperatures, T_r is approximately T_v; and in between, the rotational temperature could be some combination of T_t and T_v.

Finally, the set of calculated rate coefficients was used to extend Park's two-temperature model to a three-temperature model. The coefficients of this model were fit using a nonlinear least-squares method over three different temperature domains. When fit over the full domain of temperatures, the models performed poorly relative to the directly calculated rate coefficients. To improve the quality of the model, the temperature domain was restricted to a region where modeling T_r is critical (i.e., 13,000 to 40,000 K). In this region, the model performed well and the rms error of the fit was within 20% of the directly calculated rate coefficients. Finally, the model was refit for high temperatures ranging between 30,000 and 60,000 K, which closely matched the original data. However, at these higher temperatures, it is likely that $T_r = T_v$, and so a three-temperature model is unnecessary.

With regard to applying these results in CFD applications, using either the moderate-temperature model (13,000 to 40,000 K) or the high-temperature model (30,000 to 60,000 K) is suggested, depending on the application, but not both simultaneously. Instead, if the application experiences temperatures below 13,000 K or a wide range of temperatures ranging from 6000 to 60,000 K, interpolating

the rate coefficient on the fly during the CFD simulation is suggested. To this end, the full set of rate coefficients (including the directly calculated and interpolated rate coefficients) have been published as a supplementary data file matching the form of Table 1 alongside this paper for reference and direct substitution into CFD applications.

Appendix: Rovibrational State Probability Distributions

The rovibrational energy PDF of the reactants, $f_{rv}(\boldsymbol{n}; T_r, T_v)$, is defined as

$$f_{rv}(\boldsymbol{n}; T_r, T_v) = \prod_{i=1}^{2} f_{rv,i}(v_i, J_i; T_r, T_v) \tag{A1}$$

where $f_{rv,i}(v_1, J_1; T_r, T_v)$ denotes the rovibrational PDF of the ith reactant. The rovibrational PDF of each reactant is well defined when $T_r = T_v = T_{rv}$, i.e.,

$$f_{rv,i}(v_i, J_i; T_{rv}) = \frac{g_s(J_i)(2J_i + 1)e^{-(\epsilon_{rv}(v_i,J_i)-\epsilon_{rv}(0,0))/k_B T_{rv}}}{Q_{rv}(T_{rv})} \tag{A2}$$

where E_{rv} is the quantized rovibrational energy, g_s is the spin degeneracy, and Q_{rv} denotes the partition function. Now, decoupling T_r and T_v is not a well-defined procedure. Here, the derivation presented by Bender et al. [50], which is described as a vibration-prioritized framework, was used, and the rovibrational PDF is given by

$$f_{rv,i}(v_i, J_i; T_v, T_r) = \frac{f_{v,i}(v_i; T_v) f_{r,i}(J_i; T_r|v_i)}{\eta(T_v, T_r)} \tag{A3}$$

where $f_{v,i}$ is the vibrational PDF, $f_{r,i}$ is the rotational PDF conditioned based on the vibrational state, and η is a normalization factor. Then, $f_{v,i}$ and $f_{v,i}$ are defined by

$$f_{v,i}(v_i; T_v) = \frac{e^{-(\epsilon_{rv}(v_i,0)-\epsilon_{rv}(0,0))/k_B T_v}}{Q_v(T_v)} \tag{A4}$$

$$f_{r,i}(J_i; T_r|v_i) = \frac{g_s(J_i)(2J_i + 1)e^{-(\epsilon_{rv}(v_i,J_i)-\epsilon_{rv}(v_i,0))/k_B T_r}}{Q_{rv}(T_r)} \times \frac{1}{f_v(v_i; T_r)} \tag{A5}$$

Bender et al. [50] have shown that the normalization factor varies between 0.95 and 1.10 for a large range of T_v and T_r. Using the decoupled vibrational and rotational PDFs of each reactant, the rovibrational PDF of both reactants is given by

$$f_{rv}(\boldsymbol{n}; T_r, T_v) = \prod_{i=1}^{2} \left(\frac{f_{v,i}(v_i; T_v) f_{r,i}(J_i; T_r|v_i)}{\eta(T_v, T_r)} \right) \tag{A6}$$

Acknowledgments

This work was supported by the U.S. Air Force Office of Scientific Research under grant FA9550-12-1-0460 with Ivett Leyva as the grant monitor. The authors thank the Texas Advanced Computing Center for their generous allocation of computing time.

References

[1] Park, C., *Nonequilibrium Hypersonic Aerothermodynamics*, Wiley, New York, 1989, Chap. 3.

[2] Capitelli, M., *Molecular Physics and Hypersonic Flows*, Vol. 482, NATO Science Series C, Springer, The Netherlands, 1996, pp. 1–114, 259–406.

[3] Gnoffo, P. A., "Planetary-Entry Gas Dynamics," *Annual Review of Fluid Mechanics*, Vol. 31, Jan 1999, pp. 459–494. doi:10.1146/annurev.fluid.31.1.459

[4] Schwartz, R. N., Slawsky, Z. I., and Herzfeld, K. F., "Calculation of Vibrational Relaxation Times in Gases," *Journal of Chemical Physics*, Vol. 20, No. 10, 1952, pp. 1591–1599. doi:10.1063/1.1700221

[5] Treanor, C. E., and Marrone, P. V., "Effect of Dissociation on the Rate of Vibrational Relaxation," *Physics of Fluids*, Vol. 5, No. 9, 1962, p. 1022. doi:10.1063/1.1724467

[6] Millikan, R. C., and White, D. R., "Vibrational Relaxation in Air," *AIAA Journal*, Vol. 2, No. 10, Oct. 1964, pp. 1844–1846. doi:10.2514/3.2687

[7] Park, C., "Assessment of Two-Temperature Kinetic Model for Ionizing Air," *Journal of Thermophysics and Heat Transfer*, Vol. 3, No. 3, July 1989, pp. 233–244. doi:10.2514/3.28771

[8] Park, C., "Review of Chemical-Kinetic Problems of Future NASA Missions. 1—Earth Entries," *Journal of Thermophysics and Heat Transfer*, Vol. 7, No. 3, July 1993, pp. 385–398. doi:10.2514/3.431

[9] Knab, O., Fruehauf, H.-H., and Messerschmid, E. W., "Theory and Validation of the Physically Consistent Coupled Vibration-Chemistry-Vibration Model," *Journal of Thermophysics and Heat Transfer*, Vol. 9, No. 2, April 1995, pp. 219–226. doi:10.2514/3.649

[10] Adamovich, I. V., Macheret, S. O., Rich, J. W., and Treanor, C. E., "Vibrational Relaxation and Dissociation Behind Shock Waves. Part 1—Kinetic Rate Models," *AIAA Journal*, Vol. 33, No. 6, June 1995, pp. 1064–1069. doi:10.2514/3.12528

[11] Macheret, S. O., and Adamovich, I. V., "Semiclassical Modeling of State-Specific Dissociation Rates in Diatomic Gases," *Journal of Chemical Physics*, Vol. 113, No. 17, 2000, pp. 7351–7361. doi:10.1063/1.1313386

[12] Esposito, F., Armenise, I., Capitta, G., and Capitelli, M., "O–O_2 State-to-State Vibrational Relaxation and Dissociation Rates Based on Quasiclassical Calculations," *Chemical Physics*, Vol. 351, Nos. 1–3, July 2008, pp. 91–98.

[13] Gallis, M. A., Bond, R. B., and Torczynski, J. R., "A Kinetic-Theory Approach for Computing Chemical-Reaction Rates in Upper-Atmosphere Hypersonic Flows," *Journal of Chemical Physics*, Vol. 131, No. 12, 2009, Paper 124311. doi:10.1063/1.3241133

[14] Jaffe, R., Schwenke, D., and Chaban, G., "Theoretical Analysis of N_2 Collisional Dissociation and Rotation-Vibration Energy Transfer," *47th AIAA Aerospace Sciences Meeting*, AIAA Paper 2009-1569, Jan. 2009.

[15] Lino da Silva, M., Guerra, V., and Loureiro, J., "A Review of Non-Equilibrium Dissociation Rates and Models for Atmospheric Entry Studies," *Plasma Sources Science and Technology*, Vol. 18, No. 3, July 2009, Paper 034023. doi:10.1088/0963-0252/18/3/034023

[16] Arsentiev, I., Loukhovitski, B., and Starik, A., "Application of State-to-State Approach in Estimation of Thermally Nonequilibrium Reaction Rate Constants in Mode Approximation," *Chemical Physics*, Vol. 398, April 2012, pp. 73–80. doi:10.1016/j.chemphys.2011.06.011

[17] Panesi, M., Jaffe, R. L., Schwenke, D. W., and Magin, T. E., "Rovibrational Internal Energy Transfer and Dissociation of $N_2(^1\sum_g^+) - N(^4S_u)$ System in Hypersonic Flows," *Journal of Chemical Physics*, Vol. 138, No. 4, 2013, Paper 044312. doi:10.1063/1.4774412

[18] Munafò, A., Panesi, M., and Magin, T. E., "Boltzmann Rovibrational Collisional Coarse-Grained Model for Internal Energy Excitation and Dissociation in Hypersonic Flows," *Physical Review E*, Vol. 89, No. 2, Feb. 2014.

[19] Andrienko, D., and Boyd, I. D., "Vibrational Relaxation and Dissociation of Oxygen in Molecule-Atom Collisions," *45th AIAA Thermophysics Conference*, AIAA Paper 2015-3251, June 2015.

[20] Bender, J. D., Valentini, P., Nompelis, I., Paukku, Y., Varga, Z., Truhlar, D. G., Schwartzentruber, T., and Candler, G. V., "An Improved Potential Energy Surface and Multi-Temperature Quasiclassical Trajectory Calculations of $N_2 + N_2$ Dissociation Reactions," *Journal of Chemical Physics*, Vol. 143, No. 5, Aug. 2015, Paper 054304. doi:10.1063/1.4927571

[21] Kunova, O., Kustova, E., Mekhonoshina, M., and Nagnibeda, E., "Non-Equilibrium Kinetics, Diffusion and Heat Transfer in Shock Heated

Flows of N_2/N and O_2/O Mixtures," *Chemical Physics*, Vol. 463, Dec. 2015, pp. 70–81.
doi:10.1016/j.chemphys.2015.10.004

[22] Kulakhmetov, M., Gallis, M., and Alexeenko, A., "Ab Initio-Informed Maximum Entropy Modeling of Rovibrational Relaxation and State-Specific Dissociation with Application to the $O_2 + O$ System," *Journal of Chemical Physics*, Vol. 144, No. 17, May 2016, p. 174302.
doi:10.1063/1.4947590

[23] Kustova, E., Nagnibeda, E., Oblapenko, G., Savelev, A., and Sharafutdinov, I., "Advanced Models for Vibrational–Chemical Coupling in Multi-Temperature Flows," *Chemical Physics*, Vol. 464, Jan. 2016, pp. 1–13.
doi:10.1016/j.chemphys.2015.10.017

[24] Fiévet, R., Koo, H., and Raman, V., "Numerical Simulation of a Scramjet Isolator with Thermodynamic Nonequilibrium," *22nd AIAA Computational Fluid Dynamics Conference*, AIAA Paper 2015-3418, 2015.

[25] Fiévet, R., Voelkel, S., Koo, H., Raman, V., and Varghese, P. L., "Effect of Thermal Nonequilibrium on Ignition in Scramjet Combustors," *Proceedings of the Combustion Institute*, Vol. 36, No. 2, 2017, pp. 2901–2910.

[26] Voelkel, S. J., Raman, V., and Varghese, P. L., "Quasi-State-Specific QCT Method for Calculating the Dissociation Rate of Nitrogen in Thermal Non-Equilibrium," *54th AIAA Aerospace Sciences Meeting*, AIAA Paper 2016-0449, Jan. 2016.

[27] Candler, G. V., Olejniczak, J., and Harrold, B., "Detailed Simulation of Nitrogen Dissociation in Stagnation Regions," *Physics of Fluids*, Vol. 9, No. 7, 1997, pp. 2108–2117.
doi:10.1063/1.869330

[28] Da Silva, M. L., Guerra, V., and Loureiro, J., "State-Resolved Dissociation Rates for Extremely Nonequilibrium Atmospheric Entries," *Journal of Thermophysics and Heat Transfer*, Vol. 21, No. 1, Jan. 2007, pp. 40–49.
doi:10.2514/1.24114

[29] da Silva, M. L., Guerra, V., and Loureiro, J., "Two-Temperature Models for Nitrogen Dissociation," *Chemical Physics*, Vol. 342, Nos. 1–3, Dec. 2007, pp. 275–287.

[30] Degrez, G., Lani, A., Panesi, M., Chazot, O., and Deconinck, H., "Modelling of High-Enthalpy, High-Mach Number Flows," *Journal of Physics D: Applied Physics*, Vol. 42, No. 19, Sept. 2009, Paper 194004.
doi:10.1088/0022-3727/42/19/194004

[31] Guy, A., Bourdon, A., and Perrin, M.-Y., "Consistent Multi-Internal-Temperatures Models for Nonequilibrium Nozzle Flows," *Chemical Physics*, Vol. 420, July 2013, pp. 15–24.
doi:10.1016/j.chemphys.2013.04.018

[32] Munafò, A., Jaffe, R. L., Schwenke, D. W., and Panesi, M., "Dissociation and Energy Transfer Study of N_2–N and N_2–N_2 Interactions by Using Rovibrational and Coarse-Grained State-to-State Models," *53rd AIAA Aerospace Sciences Meeting*, AIAA Paper 2015-0480, Jan. 2015.

[33] Jaffe, R., Schwenke, D., and Chaban, G., "Vibration-Rotation Excitation and Dissociation in N_2–N_2 Collisions from Accurate Theoretical Calculations," *10th AIAA/ASME Joint Thermophysics and Heat Transfer Conference*, AIAA Paper 2010-4517, June–July 2010.

[34] Kim, J. G., and Boyd, I. D., "State-Resolved Master Equation Analysis of Thermochemical Nonequilibrium of Nitrogen," *Chemical Physics*, Vol. 415, March 2013, pp. 237–246.
doi:10.1016/j.chemphys.2013.01.027

[35] Kunova, O., and Nagnibeda, E., "State-to-State Description of Reacting Air Flows Behind Shock Waves," *Chemical Physics*, Vol. 441, Sept. 2014, pp. 66–76.
doi:10.1016/j.chemphys.2014.07.007

[36] Esposito, F., Armenise, I., and Capitelli, M., "N–N_2 State to State Vibrational-Relaxation and Dissociation Rates Based on Quasiclassical Calculations," *Chemical Physics*, Vol. 331, No. 1, Dec. 2006, pp. 1–8.
doi:10.1016/j.chemphys.2006.09.035

[37] Chaban, G., Jaffe, R., Schwenke, D., and Huo, W., "Dissociation Cross Sections and Rate Coefficients for Nitrogen from Accurate Theoretical Calculations," *46th AIAA Aerospace Sciences Meeting and Exhibit*, AIAA Paper 2008-1209, Jan. 2008.

[38] Schwenke, D. W., "Dissociation Cross Sections and Rates for Nitrogen," Non-Equilibrium Gas Dynamics-From Physical Models to Hypersonic Flights TR RTO-EN-AVT-162, Rhode St. Genèse, Belgium, 2009.

[39] Andrienko, D. A., and Boyd, I. D., "Rovibrational Energy Transfer and Dissociation in O_2–O Collisions," *Journal of Chemical Physics*, Vol. 144, No. 10, March 2016, Paper 104301.
doi:10.1063/1.4943114

[40] Candler, G. V., and MacCormack, R. W., "Computation of Weakly Ionized Hypersonic Flows in Thermochemical Nonequilibrium," *Journal of Thermophysics and Heat Transfer*, Vol. 5, No. 3, July 1991, pp. 266–273.
doi:10.2514/3.260

[41] Park, C., "The Limits of Two-Temperature Kinetic Model in Air," *48th AIAA Aerospace Sciences Meeting*, AIAA Paper 2010-0911, Jan. 2010.

[42] Voelkel, S., Raman, V., and Varghese, P. L., "Effect of Thermal Nonequilibrium on Reactions in Hydrogen Combustion," *Shock Waves*, Vol. 26, No. 5, March 2016, pp. 539–549.
doi:10.1007/s00193-016-0645-0

[43] Valentini, P., Norman, P., Zhang, C., and Schwartzentruber, T. E., "Rovibrational Coupling in Molecular Nitrogen at High Temperature: An Atomic-Level Study," *Physics of Fluids*, Vol. 26, No. 5, May 2014, Paper 056103.
doi:10.1063/1.4875279

[44] Bender, J. D., Nompelis, I., Valentini, P., Doraiswamy, S., Schwartzentruber, T. E., Candler, G. V., Paukku, Y., Yang, K. R., Varga, Z., and Truhlar, D. G., "Quasiclassical Trajectory Analysis of the $N_2 + N_2$ Reaction Using a New Ab Initio Potential Energy Surface," *11th AIAA/ASME Joint Thermophysics and Heat Transfer Conference*, AIAA Paper 2014-2964, June 2014.

[45] Porter, R. N., and Raff, L. M., "Classical Trajectory Methods in Molecular Collisions," *Dynamics of Molecular Collisions: Part B*, edited by W. H. Miller, Vol. 2, Modern Theoretical Chemistry, Plenum Press, New York, 1976, pp. 1–50.

[46] Truhlar, G., and Muckerman, J. T., "Reactive Scattering Cross Sections III: Quasiclassical and Semiclassical Methods," *Atom-Molecule Collision Theory: A Guide for the Experimentalist*, edited by R. B. Bernstein, Plenum Press, New York, 1979, pp. 505–566.

[47] Levine, R. D., *Molecular Reaction Dynamics*, Cambridge Univ. Press, New York, 2005, pp. 148–196.

[48] Henriksen, N. E., and Hansen, F. Y., *Theories of Molecular Reaction Dynamics: The Microscopic Foundation of Chemical Kinetics*, Oxford Graduate Texts, Oxford Univ. Press, Oxford, 2012, pp. 20–26.

[49] Prince, P., and Dormand, J., "High Order Embedded Runge–Kutta Formulae," *Journal of Computational and Applied Mathematics*, Vol. 7, No. 1, March 1981, pp. 67–75.
doi:10.1016/0771-050X(81)90010-3

[50] Bender, J. D., Valentini, P., Nompelis, I., Schwartzentruber, T. E., and Candler, G. V., "Characterization of Vibrational and Rotational Energy Transfer in $N_2 + N_2$ Dissociative Collisions Using the Quasiclassical Trajectory Method," *45th AIAA Thermophysics Conference*, AIAA Paper 2015-3253, June 2015.

[51] Paukku, Y., Yang, K. R., Varga, Z., and Truhlar, D. G., "Global Ab Initio Ground-State Potential Energy Surface of N_4," *Journal of Chemical Physics*, Vol. 139, No. 4, 2013, Paper 044309.
doi:10.1063/1.4811653

[52] Henkelman, G., and Jónsson, H., "Improved Tangent Estimate in the Nudged Elastic Band Method for Finding Minimum Energy Paths and Saddle Points," *Journal of Chemical Physics*, Vol. 113, No. 22, 2000, pp. 9978–9985.
doi:10.1063/1.1323224

[53] Henkelman, G., Uberuaga, B. P., and Jónsson, H., "A Climbing Image Nudged Elastic Band Method for Finding Saddle Points and Minimum Energy Paths," *Journal of Chemical Physics*, Vol. 113, No. 22, 2000, pp. 9901–9904.
doi:10.1063/1.1329672

[54] Wang, Q., Moin, P., and Iaccarino, G., "A High Order Multivariate Approximation Scheme for Scattered Data Sets," *Journal of Computational Physics*, Vol. 229, No. 18, Sep 2010, pp. 6343–6361.
doi:10.1016/j.jcp.2010.04.047

[55] Hanson, R. K., and Baganoff, D., "Shock-Tube Study of Nitrogen Dissociation Rates Using Pressure Measurements," *AIAA Journal*, Vol. 10, No. 2, Feb. 1972, pp. 211–215.
doi:10.2514/3.50082

[56] Kewley, D., and Hornung, H., "Free-Piston Shock-Tube Study of Nitrogen Dissociation," *Chemical Physics Letters*, Vol. 25, No. 4, April 1974, pp. 531–536.
doi:10.1016/0009-2614(74)85360-1

[57] Gonzales, D. A., and Varghese, P. L., "Evaluation of Simple Rate Expressions for Vibration-Dissociation Coupling," *Journal of Thermophysics and Heat Transfer*, Vol. 8, No. 2, April 1994, pp. 236–243.
doi:10.2514/3.529

[58] Gonzales, D. A., and Varghese, P. L., "Vibrational Relaxation Models for Dilute Shock Heated Gases," *Chemical Physics*, Vol. 195, Nos. 1–3, June 1995, pp. 83–91.
doi:10.1016/0301-0104(95)00078-3